International Journal of Chemical, Materials and Biomolecular Sciences
ISSN: 2415-6620
Vol:14, No:1, 2020

Effective Photodegradation of Tetracycline by a Heteropoly Acid/Graphene Oxide Nanocomposite Based on Uio-66

Anasheh Maridiroosi, Ali Reza Mahjoub, Hanieh Fakhri

***Abstract*—**Heteropoly acid nanoparticles anchored on graphene oxide based on UiO-66 were synthesized via in-situ growth hydrothermal method and tested for photodegradation of a tetracycline as critical pollutant. Results showed that presence of graphene oxide and UiO-66 with high specific surface area, great electron mobility and various functional groups make an excellent support for heteropoly acid and improve photocatalytic efficiency up to 95% for tetracycline. Furthermore, total organic carbon (TOC) analysis verified 79% mineralization of this pollutant under optimum condition.

***Keywords*—**Heteropoly acid, graphene oxide, MOF, tetracycline.

I. Introduction

AROUND the world, environmental problems become serious concerns. Majority of pollutants have high solubility in aqueous solution and eventually threat human health. The World Health Organization (WHO) has considered tetracycline (TC) as one of the most dangerous pollutants [1]. TC is one of the cheapest and commonly used antibiotics. The ecological risk caused by TC has been identified and intensive efforts have also been devoted to treat this polluted solution. The occurrence of TC in the environment can induce genetic exchange, resistance of bacteria against drugs, and subsequently threat to human health [2], [3]. With this background, nowadays, the removal of this toxic pollutant is considered as a hot issues being investigated.

In recent years, heterogeneous photocatalysis has emerged as a promising method to remove of various pollutants due to its simplicity, low cost and reusability [4]. This process is done by numerous nanomaterials such as metal oxide [5], [6], calcogenide [7], provskite [8] etc.

In the past few years, heteropoly acids (HPAs) with a special structural feature attracted more attention in photocatalytic systems [9]. HPAs are formed of a particular combination of hydrogen and oxygen with certain metals and non-metals. These compounds represent good photo oxidizing characters that are in favor in photocatalytic system [10]. Among HPAs, Keggin-type with the formula $[XM_{12}O_{40}]^{n-}$, where X can be the heteroatom such as P^{5+} or Si^{4+} and M selected typically W or Mo with high oxidation state, has been mostly used as photocatalyst [11]. However, high solubility in aqueous solution and low surface area limit their vast application. It has been reported by the several researches that immobilizing of HPAs on layer of graphene oxide (GO) can make heterogeneous photocatalyst with improved efficiency [12], [13], although, high stacking and low empirical surface area of GO are drawbacks that should be solved.

Recently, composites containing GO based on metal-organic frameworks (MOFs) appeared as a new type of used platform in photocatalytic system that led to enhance the photocatalytic activity [14]-[17]. Enhanced photodegradation of amoxyciline achieved by using MIL-68(In)/GO composite is reported by Yang et al. [18]. In another study, the Ce doped UiO-66/GO nanocomposite indicted improved photoreduction of nitrocompounds in the green catalytic route [19]. Indeed, the composite containing GO and MOF supplies the compact design of atoms, various oxygen functionalities, proper dispersivity of MOF, low stacking of GO and high surface area. However, so far, relatively little attention has been paid to ternary composite containing HPAs functionalized GO-based MOF to form visible-light-driven photocatalysts. Here, we report a facile approach for preparation of this ternary nanocomposite $H_3PMo_4W_8O_{40}$/GO based on UiO-66 (MWGU) and assay its performance in photodegradation of TC. This work can introduce strategy for the development of MOF based materials with high photocatalytic activity.

II. Materials and Methods

A. Materials

All of the chemicals were purchased from Merck and Aldrich and used without further purification.

B. Synthesis of $H_3PMo_8W_4O_{40}$/GO

H3PMo8W4O40 (MW) was synthesized by procedure of Huixiong et al. [20] and the modified Hummers method is employed to synthesis of GO [21]. In the following, for the synthesis of H3PMo8W4O40/GO (MWG), 0.7 g of MW was dispersed in 20 ml HCl and then 1 g of GO was added to it. The mixture was stirred for 30 min at room temperature. Then, it was moved to autoclave and kept at 140℃ for 24 h. The precipitate was separated using centrifuge machine and washed by ethanol and dionized water for several times. Finally, MWG sample was obtained when it was dried at 80 ℃ for 8 h. The obtained result of ICP analysis indicated that 30% of MW is loaded on GO layers.

Anasheh Mardiroosi, Ali Reza Mahjoub, and Hanieh Fakhri are with the Department of Chemistry, Tarbiat Modares University, P.O. Box. 14155-4383 Tehran, Iran (e-mail: a.mardiroosi@gmail.com, mahjouba@modares.ac.ir, hanieh_fakhrie@yahoo.com).

C. Synthesis of Uio-66

To synthesize UiO-66, ZrCl4 (0.38 g) and terephthalic acid (H2BDC) (0.27 g) were suspended in 20 ml dimethylformamide (DMF) and transferred to teflon-lined autoclave and maintained at 120 °C for 24 hours [22]. Then, the collected powder was filtered by centrifugation and following washed with DMF and methanol for three times. Finally, it was dried at 120℃ for 12 h.

D. Synthesis of MWGU

In this procedure, 0.12 g MWG was dissolved in 20 ml DMF and after being sonication for 6 h, 0.38 g ZrCl4 was added to it and stirred for 30 min. Then, 0.27 g H2BDC was added to mixture. The suspension was placed at 120℃ for 24 h. After washing by DMF, the product was dried at 120℃ for 24 h. In here, the MWG ratio was calculated as:

$$\text{MWG ratio\%} = \text{MWG mass/total mass } (ZrCl_4 \text{ mass} + H_2BDC \text{ mass} + \text{MWG mass}) \quad (1)$$

According to (1), MWG ratio was achieved 15%, so this product was labeled 15MWGU. The other percentages were prepared using a similar method.

E. Photocatalytic Activity

The photocatalytic activity of photocatalysts was investigated for photodegradation of TC using visible light source (Hg lamp (500W, λ > 400 nm). To evaluate the photoactivity, the photocatalysts (0.02 g) were suspended in 50 ml of pollutant solution (20 ppm). During the experiment, an aliquot of the solution was taken at 15 min interval and monitored at 373 nm using UV-Vis spectrophotometer (Shimadzu UV 2100). The effect of pH was investigated by altering pH from 2 to 9 using HCl and NaOH (1 M).

The photocatalytic efficiency was calculated according to:

$$\text{Photocatalytic efficiency}(\%) = \frac{(Co-Ce)}{C_0} * 100 \quad (2)$$

where C_0 and C_e are the initial and equilibrium concentration of the pollutant (mg. L^{-1}).

F. Characterization

The FT-IR spectra were obtained by a thermo Scientific Nicolet IR100 (Madison, WI) Fourier transform infrared (FT-IR) spectrometer. The morphology of synthesized samples was characterized by scanning electron microscopy (SEM, Philips XL-300 instrument) and Transmission electron microscopy (TEM, Philips EM208S 100KV). The purity phase and crystalline structure were assayed using powder X-ray diffraction (XRD) on Philips X-pert X-ray diffractometer using Cu Kα radiation (wavelength, λ = 1.5418 ˚A). The photocatalytic efficiency was investigated using UV-Vis spectrophotometer (Shimadzu-UV-2550-8030) in the range of 200-800 nm at room temperature. TOC analyzer (Shimadzu, TOC analyzer –VCSH Model) was employed for calculating the mineralization of pollutant.

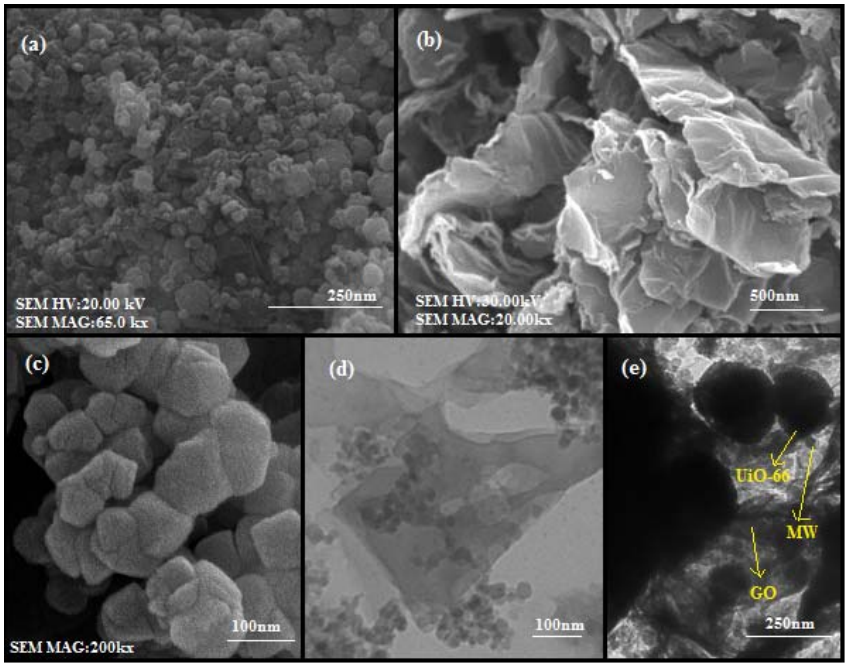

Fig. 1 SEM images of MW (a), GO (b), UiO-66 (c) and TEM images of MWG (d) and MWGU (e)

III. Result and Discussion

The morphology and texture of samples were assayed by SEM and TEM analysis. Fig. 1 (a) illustrates MW sample with nanoparticle morphology in the size of about 35-40 nm. The smooth and silk-like sheets for GO sample were indicated in Fig. 1 (b). As shown (Fig. 1 (c)), the prepared UiO-66 sample

indicates octahedral structure with the size distribution in range of 100-150 nm. TEM image in Fig. 1 (d) confirmed the strong attachment of MW nanoparticles on GO layers. It can be seen in Fig. 1 (e) that octahedral of UiO-66 was grown on the surface of MWG sheets which could indicate a well contact among the three components.

Fig. 2 A indicates FT-IR spectra of products. For MW sample, four main peaks the peaks at 1060-1080 cm^{-1} (P-O), 967-978 cm^{-1} (M=O), 870-880 cm^{-1} (Mo-O-Mo) and 770-780 cm^{-1} (Mo-O-Mo) are observed in Fig. 2 (a) that are similar with previous report [20]. Moreover, the broad band approximately 3200-3400 cm^{-1} is attributed to the hydroxyl groups [23]. In the spectra of UiO-66 sample (Fig. 2 (b)), the observed band at 430-700 cm^{-1} is corresponded to combination of Zr–O modes with OH and CH bending vibration [24]. Furthermore, the located bands at 1612 and 1730 cm^{-1} are attributed to the stretching vibration of conjugated C=C of benzene ring and C=O stretching vibration [25]. For GO sample (Fig. 2 (c)), characteristic bands at 1714, 1632, 1254 and 1081 cm^{-1} are referred to C=O, C=C, O-C-O and C-OH stretching vibrations [26]. Fig 2 (d) illustrates the main characteristic peaks belong to MW [27], GO and UiO-66 that confirmed successful formation of nanocomposite.

Fig 3 (a) presents UV–Vis absorption spectra of MW and MWGU. Absorption spectra of MW indicated a red-shift of adsorption edge in comparison with MWGU. The calculated band gaps are 2.9 eV for MW and 2.6 eV for MWGU. These data revealed significant influence of UiO-66 and GO on the optical properties of MW.

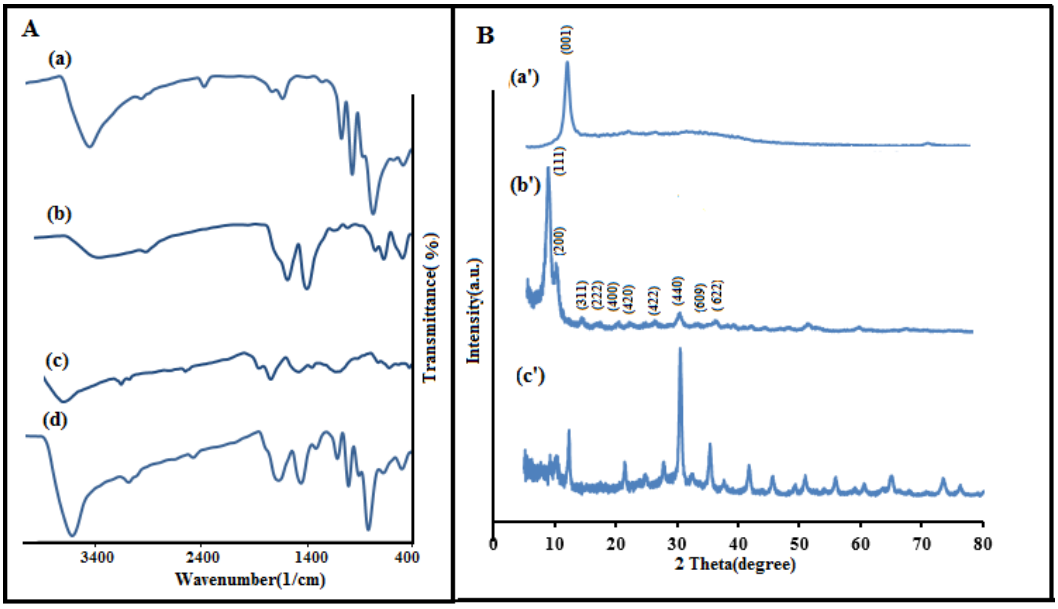

Fig. 2 Section A: FT-IR spectra of MW (a), UiO-66 (b), GO (c) and MWGU (d); section B: XRD patterns of GO (a'), UiO-66 (b') and MWGU (c')

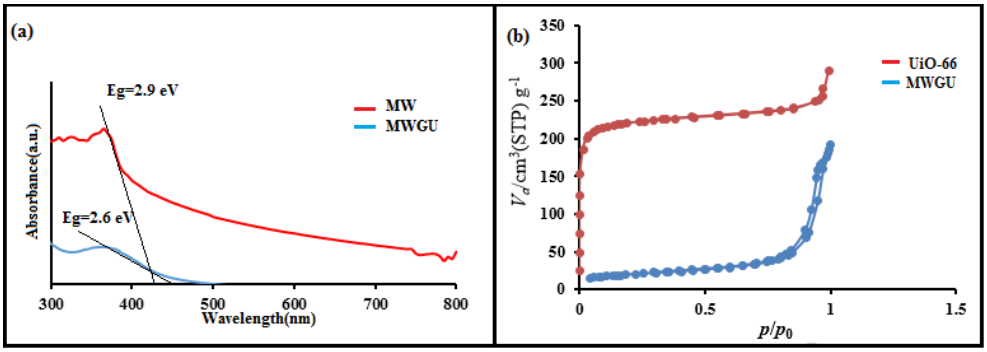

Fig. 3 UV–Vis spectra of MW and MWGU (a); N_2 adsorption-desorption isotherms of samples (b)

To investigate surficial characters of products, N_2 adsorption/desorption technique was used. The Brunauer–Emmett–Teller equation (BET) is employed for determination of surface area. As seen in Fig. 3 (b), the specific surface area was achieved 856 m^2/g for pure UiO-66 and reduced to 70.06 m^2/g for MWGU. This change can be attributed to blocking of pores belong to UiO-66 by MWG. Furthermore, both curves indicated a type-IV isotherm which corresponded to their

mesoporous properties. After UiO-66 modification, the size of pores is enlarged (Table I). This increase referred to new crystallization site for UiO-66 by entrance of MWG [28].

IV. Photocatalytic Degradation

A. The Control Experiments

At first, control experiments were applied for investigation of photocatalyst and light irradiation effects on pollutant degradation (Fig. 4 (a)). In the dark condition, only 15% of TC removed that are attributed to adsorption of them by functional groups belonging to GO and UiO-66. In other experiment, stability of pollutants under visible light irradiation without any photocatalyst was investigated. Photolysis efficiency was obtained about 6% for TC after 120 min irradiation. Hence, degradation of these pollutants needs to stimulus presence of light and photocatalyst.

TABLE I
Surface Area and Average Pore Size Distribution of Samples

Samples	BET surface area(m^2/g)	Average pore diameters (nm)
UiO-66	856.61	2.07
MWGU	70.06	15.8

B. The Effect of MWG Dosage

Fig. 4 (b) shows the photocatalytic activity of MWGU nonocomposite with various mass ratio of MWG. In the first, more efficiency is obtained along with increase of MWG dosage. When the 35MWGU is used, the maximum photodegradation can be achieved. So this ratio is elected as an optimum photocatalyst. The further increase of dosage leads to reduction efficiency that may be due to vast agglomeration of MW nanoparticles. It can be found from Fig. 4 (c) that 26% of the TC solution can be removed under 120 min irradiation by the pure MW photocatalyst while results indicated an enhanced photocatalytic activity with introducing of GO and UiO-66.

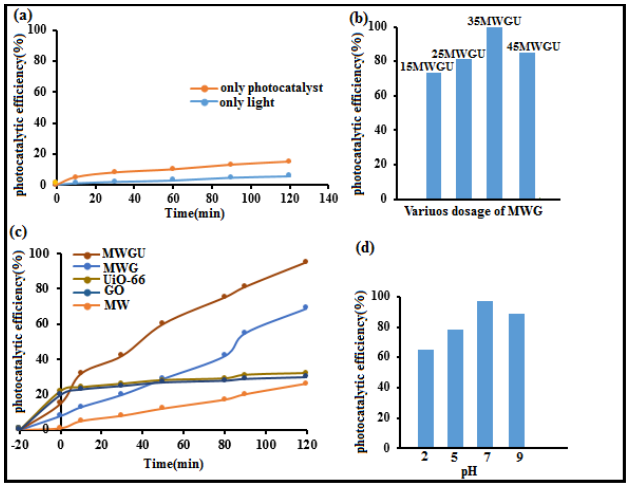

Fig. 4 Dependence of photodegradation of TC to the presence of light and photocatalyst (a), the photocatalytic efficiency by various loading of MWG (b), the photocatalytic efficiency by various photocatalyst (c), The effect of pH solution on the photocatalytic efficiency for photodegradation of TC (d)

C. The Effect of pH

The initial pH of solution plays important role in determining nature of photocatalyst. As shown in Fig. 4 (d), the removal of TC increases along with increasing the pH from 2 until 7. For a higher pH, it is seen that efficiency is decreased. In the acidic pH, the Cl^- ions (following in acidification by HCl) can react with OH radical that resulted to produce inorganic ClO anion radical. ClO^- radical has a lower activity than OH radical and decreased efficiency is expectable [29]. In the higher pH (pH > 7), the repulsive electrostatic force between deprotonated TC and negative surface of photocatalyst lead to decline of efficiency. Hence, pH of 7 was considered as the optimized value.

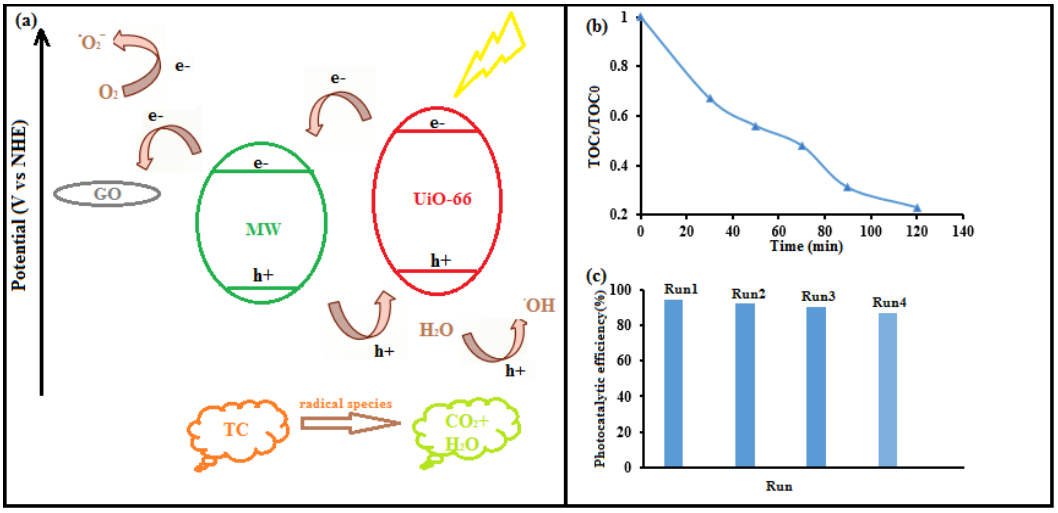

Fig. 5 The possible mechanism of photodegradation by synthesized photocatalyst under visible light irradiation (a), mineralization of TC in the photocatalytic process as a function of contact time (b); photocatalytic efficiency over four consecutive cycles (c)

D.Study of the Nature of the Photodegradation

After irradiation using visible light source, UiO-66 and MWG were excited to produce electron-hole pairs. As the LOMO potential of UiO-66 is more negative than conductive potential of used MW [30], [31], the photoinduced electrons migrate from LOMO belong to UiO-66 to conductive band of MW and reversely, holes transfer from valance band of HPAs to HOMO of UiO-66 (Fig. 5 (a)). Here, UiO-66 improves the adsorption of visible light and GO acts as acceptor substrate toward transfer of photogenerated electron and declines recombination rate of charge carriers.

Fig. 5 (b) represents mineralization efficiency by 35MWGU. The maximum mineralization of TC was achieved 79%. This different percentage between mineralization and photocatalytic efficiency is referred to presence of intermediates of pollutants oxidation that can be mineralized by using continue of reaction at the longer time. In order to evaluate the reusability of photocatalyst, ethanol solution was selected as elution solvent. The recycled photocatalyst indicated reasonable efficiency after four consecutive cycles as shown in Fig. 5 (c). These results revealed that these nanocomposites have a good potential as cost-effective photocatalyst for pollutant removal.

V. Conclusion

In summary, a ternary MWG based on UiO-66 photocatalyst was successfully synthesized via in-situ growth hydrothermal method. The photocatalytic performance showed that MWGU exhibited higher activity than pure MW and GO in the degradation of TC, attributed to higher surface area, the presence of various functional groups and a red-shift of adsorption edge for MWGU. The best result of photocatalytic activity (95% removal of TC respectively under visible light irradiation) is obtained for 35MWGU. All experiments show that this nanocomposite can be appointed as a good photocatalyst in visible light area.

Acknowledgment

Support of this investigation by Tarbiat Modares University and Iranian nanotechnology initiative council is gratefully acknowledged.

References

[1] WHO. Guidelines for Drinking Water Quality, Vol 1: Recommendations, 2nd ed. WHO: Geneva, 1993.
[2] Niu J, Ding S, Zhang L, Zhao J, Feng C. Visible-light-mediated Sr-Bi2O3 Mboula photocatalysis of tetracycline: kinetics, mechanisms and toxicity assessment. Chemosphere. 2013; 93: 1–8.
[3] V.M, Hequet V, Gru Y, Colin R, Andres, Y. Assessment of the efficiency of photocatalysis on tetracycline biodegradation. J. Hazard. Mater. 2012; 209: 355–364.
[4] Zhang Q, Lima D.Q, Lee I, Zaera F, Chi M.F, Yin Y.D, J. Angew. Chem. Int. Ed. 2010; 123: 7226–7230.
[5] Ghorbanpour M, Hakimi B, Feizi A. A Comparative Study of Photocatalytic Activity of ZnO/activated Carbon Nanocomposites Prepared by Solid-state and Conventional Precipitation Methods. J Nanostruct. 2018; 8: 259-265.
[6] Hassanpour M, Salavati-Niasari M, Mousavi S.A. Safardoust-Hojaghan H, Hamadanian M, CeO2/ZnO Ceramic Nanocomposites, Synthesized via Microwave Method and Used for Decolorization of Dye. J Nanostruct. 2018; 8: 97-106.
[7] Yan Y, Yang M, Shi H, Wang C, Fan J, Liu E, Hu X, CuInS2 sensitized TiO_2 for enhanced photodegradation and hydrogen production. Ceram Inter. 2019; 45: 6093-6101.
[8] Dhiman M, Tripathi M, Singhal S, Structural, optical and photocatalytic properties of different metal ions (Cr3+, Co2+, Ni2+, Cu2+ and Zn2+) substituted quaternary perovskites. Mater Chem Phys. 2107; 202: 40-49
[9] Taghavi M, Ehrampoush M.H, Ghaneian M.T, Tabatabaee M, Fakhri Y, Application of a Keggin-type heteropoly acid on supporting nanoparticles in photocatalytic degradation of organic pollutants in aqueous solutions. J Clean Prod. 2018;197: 1447-1453.
[10] Shahrnoy A.A, Mahjoub A.R, Morsali A, Dusek M, Eigner V. Sonochemical synthesis of polyoxometalate based of ionic crystal nanostructure: A photocatalyst for degradation of 2, 4-dichlorophenol. Ultrason sonochem. 2018; 40: 174-183.
[11] Mohebali H, Abolhosseini Shahrnoy A, Mahjoub A.R, Effect of substituting molybdenum atoms with tungsten on photocatalyst activity of cesium salt of keggin type polyoxometalates decorated magnetic ceria, Journal of Molecular Structure.
[12] Yang H, Liu X, Sun S, Nie Y, Wu H, Yang T, Zheng S, Lin S, Green and facile synthesis of graphene nanosheets/K3PW12O40 nanocomposites with enhanced photocatalytic activities. Mater Res Bull. 2016; 78: 112-118
[13] Fakhri H, Mahjoub A.R, Aghayan H. Effective removal of methylene blue and cerium by a novel pair set of heteropoly acids based functionalized graphene oxide: Adsorption and photocatalytic study. Chem eng res des. 2017; 120: 303–315.
[14] Furukawa H, Yaghi OM and at al. The Chemistry and Applications of Metal-Organic Frameworks. Science. 2013; 341:1230444
[15] Zhou HC, Long JR, Yaghi OM. Introduction to Metal–Organic Frameworks. Chem Rev. 2012; 112:673–674.
[16] Xie MH, Shao R, Xi XG, Hou GH, Guan RF, Dong PY, Zhang QF, Yang XL. Metal–Organic Framework Photosensitized TiO_2 Co-catalyst: A Facile Strategy to Achieve a High Efficiency Photocatalytic System. Chem Eur J. 2017; 23:3931–3937.
[17] Zhao XH, Liu X, Zhang ZY, Liu X, Zhang W. Facile preparation of a novel SnO2@UiO-66/rGO hybrid with enhanced photocatalytic activity under visible light irradiation. RSC Adv 2016; 6: 92011–92019.
[18] Yang C, You X, Cheng J, Zheng H, Chena Y. A novel visible-light-driven In-based MOF/graphene oxide composite photocatalyst with enhanced photocatalytic activity toward the degradation of amoxicillin. Appl Catal B Environ. 2017; 200: 673–680.
[19] Yang Z, Xu X, Liang X, Lei C, Gao L, Hao R, Lu D, Lei Z. Fabrication of Ce doped UiO-66/Graphene Nanocomposites with Enhanced Visible Light Driven Photoactivity for Reduction of Nitroaromatic Compounds. Appl Surf Sci. 2017; 420: 276-285.
[20] Huixiong W, Mei Z, Yixin Q, Haixia L, Hengbo Y. Preparation and characterization of tungsten-substituted molybdophosphoric acids and catalytic cyclodehydration of1,4-butanediol to tetrahydrofuran. Chin. J. Chem. Eng. 2009; 17: 200–206.
[21] William H, Offeman R.E, Preparation of graphene oxide. Amer J, Chem. Soc. 1958; 80: 1339.
[22] Ding J, Yang Z, He C, Tong X, Li Y, Niu X, Zhang H. UiO-66 (Zr) coupled with Bi2MoO6 as photocatalyst for visible-light promoted dye degradation. J Colloid Interf Sci. 2017;1: 126-133.
[23] Abolhosseini A, Mahjoub A.R, Eslami-Moghadam M, Fakhri H. Dichloro (1,10-phenanthroline-5,6-dione) palladium (II) complex supported by mesoporous silica SBA-15 as a photocatalyst for degradation of 2,4-dichlorophenol. J Mol Struct. 2014; 1076: 568–575.
[24] Yao P, Liu H, Wang D, Chen J, Li G, An T. Enhanced visible-light photocatalytic activity to volatile organic compounds degradation and deactivation resistance mechanism of titania confined inside a metal-organic framework. J Colloid Interf Sci. 2018; 522: 174-182.
[25] Nantao H, Zhi Y, Yanyan W, Liling Z, Ying W, Xiaolu H, Hao W, Liangmin W, and Zhang Y. Ultrafast and sensitive room temperature NH_3 gas sensors based on chemically reduced graphene oxide. Nanotechnology. 2014; 25:025502.
[26] Fakhri H, Mahjoub A.R, CheshmeKhavar A.H. Improvement of visible light photocatalytic activity over graphene oxide/$CuInS_2$/ZnO nanocomposite synthesized by hydrothermal method. Mater Sci Semicon Proc. 2016; 41: 38–44.
[27] Chandrasekaran S, Choi WM, Chung JS, Hur SH, Kim EJ. 3D crumpled RGO-Co3O4 photocatalysts for UV-induced hydrogen evolution reaction. Mater Lett. 2014; 136:118–121.
[28] Zhou X, Huang W, Shi J, Zhao Z, Xia Q, Li Y, Wang H, Li Z. A novel

MOF/graphene oxide composite GrO@ MIL-101 with high adsorption capacity for acetone. J Mater Chem A. 2014; 2: 4722-4730.

[29] Nezamzadeh-Ejhieh A, Shirzadi A. Enhancement of the photocatalytic activity of Ferrous Oxide by doping onto the nano-clinoptilolite particles towards photodegradation of tetracycline. Chemosphere. 2014; 107:136–144.

[30] Shi H, Yu Y, Zhang Y, Feng X, Zhao X, Tan H, Ullah Khan S, Li Y, Wang E, Polyoxometalate/TiO2/Ag composite nanofibers with enhanced photocatalytic performance under visible light. Appl Catal B Environ. 2018; 221: 280-289.

[31] Ling L, Wang Y, Zhang W, Ge Z, Duan W, Liu B. Preparation of a Novel Ternary Composite of TiO_2/UiO-66-NH_2/ Graphene Oxide with Enhanced Photocatalytic Activities. Catal Lett. 2018; 148:1978-1984.